Characterization of the sulphate mineral coquimbite, a secondary iron sulphate from Javier Ortega mine, Lucanas Province, Peru – Using infrared, Raman spectroscopy and thermogravimetry

Ray L. Frost [a],*, Željka Žigovečki Gobac [b], Andrés López [a], Yunfei Xi [a], Ricardo Scholz [c], Cristiano Lana [c], Rosa Malena Fernandes Lima [d]

[a] School of Chemistry, Physics and Mechanical Engineering, Science and Engineering Faculty, Queensland University of Technology, GPO Box 2434, Brisbane, Queensland 4001, Australia
[b] Institute of Mineralogy and Petrography, Department of Geology, Faculty of Science, University of Zagreb, Horvatovac 95, 10000 Zagreb, Croatia
[c] Geology Department, School of Mines, Federal University of Ouro Preto, Campus Morro do Cruzeiro, Ouro Preto, MG 35400-00, Brazil
[d] Mining Engineering Department, School of Mines, Federal University of Ouro Preto, Campus Morro do Cruzeiro, Ouro Preto, MG 35400-00, Brazil

HIGHLIGHTS

- We have studied the mineral coquimbite.
- Using SEM with EDX, thermal analytical techniques and Raman and infrared spectroscopy.
- Chemical formula was determined as $(Fe^{3+}_{1.37}, Al_{0.63})_{\sum 2.00}(SO_4)_3 \cdot 9H_2O$.
- Thermal analysis showed a total mass loss of ~73.4% on heating to 1000 °C.

ARTICLE INFO

ABSTRACT

The mineral coquimbite has been analysed using a range of techniques including SEM with EDX, thermal analytical techniques and Raman and infrared spectroscopy. The mineral originated from the Javier Ortega mine, Lucanas Province, Peru. The chemical formula was determined as $(Fe^{3+}_{1.37}, Al_{0.63})_{\sum 2.00}(SO_4)_3 \cdot 9H_2O$. Thermal analysis showed a total mass loss of ~73.4% on heating to 1000 °C. A mass loss of 30.43% at 641.4 °C is attributed to the loss of SO_3. Observed Raman and infrared bands were assigned to the stretching and bending vibrations of sulphate tetrahedra, aluminium oxide/hydroxide octahedra, water molecules and hydroxyl ions. The Raman spectrum shows well resolved bands at 2994, 3176, 3327, 3422 and 3580 cm^{-1} attributed to water stretching vibrations. Vibrational spectroscopy combined with thermal analysis provides insight into the structure of coquimbite.

© 2014 Elsevier B.V. All rights reserved.

1. Introduction

Coquimbite is an iron (III) sulphate mineral of ideal formula $Fe^{3+}_2(SO_4)_3 \cdot 9H_2O$, which derives its name from the Coquimbo region, Chile [1]. Coquimbite is found as secondary mineral developed in the oxidized portions of weathering iron sulphide deposits in arid regions, although it could be also found associated with fumarolic activity [1]. The mineral was first described from Tierra Amarilla near Copiapó, Chile [2–5], and other occurrences were reported in Quetena, Chuquicamata, Alcaparrosa, Chile; Concepción mine, Huelva, Spain; Skouriotisa, Cyprus; Rammelsberg, Hartz, Germany, among others [1,3,6–8].

Coquimbite was recently found in Peru, at the Javier Ortega mine, Lucanas Province, Departmento Ayacucho [9]. Main ore mineral in Javier Ortega mine is chalcopyrite and secondary ore minerals are sphalerite and galena [9]. Coquimbite occurs in the oxidized portions of this iron sulphide deposit, together with other secondary sulphate minerals like alunogen, chalcanthite, copiapite, halotrichite, jarosite, krausite, römerite and with sulphur. Coquimbite in Javier Ortega mine occurs in well developed violet crystals up to 5 cm long [9].

Coquimbite is a hexagonal mineral [10,11] with $a = 10.922(9)$, $c = 17.084(14)$ Å, space group $P\bar{3}1c$ and $Z = 4$ [12]. Ideal formula of this mineral is $Fe^{3+}_2(SO_4)_3 \cdot 9H_2O$, but there is often a replacement of Fe^{3+} by Al^{3+}, so the formula of this mineral should be written $Fe^{3+}_{2x}Al_x(SO_4)_3 \cdot 9H_2O$ [6,12]. There are three outstanding features of the coquimbite structure. The dominant structural

---

feature is a discontinuous chain, composed of alternating Fe octahedra and S tetrahedra, parallel to, and approximately one-half the length of, the c axis. The symmetry causes the chain to be repeated in the upper one-half of the cell. The individual chain segments (i.e. two centrosymmetrically related clusters of six SO_4 tetrahedra and three Fe octahedra in each unit cell) are linked through hydrogen bonds only. The second structural feature is the geometrical arrangement of these chains which gives rise to "channels", paralleling the a_1 and a_2 axes, which are occupied by water molecules linked to the chains by hydrogen bonds. The third structural feature are independent (Al, Fe) octahedra located at the origin and at the centre of the c edges surrounded by six H_2O molecules. There are three crystallographically different iron atoms octahedrally coordinated to six O and/or Ow (= oxygen atom of an H_2O molecule) forming $Fe1O4_6$, $Fe2O3_3Ow3_3$, and $Fe3Ow1_6$ octahedra. Two of in total three crystallographically independent H_2O molecules, Ow1 and Ow3 are bonded to one iron atom, whereas Ow2 is not bonded to any cation. The mean ⟨Fe–O⟩ distance of Fe3 site differ from distances of Fe1 and Fe2 sites, and such a difference in average bond distance can be attributed to the partial Fe3 site occupation also by Al atoms. So, the crystal structure of coquimbite could be described as a $[Fe_4(H_2O)_{12}(SO_4)_6]^0$ framework consisting of $[Fe1Fe2_2(H_2O)_6(SO_4)_6]^{3-}$ clusters and isolated $[Fe3(H_2O)_6]^{3+}$ octahedra connected to each other only by hydrogen bonds. Ow1 and Ow3 atoms are engaged in the further interconnection of the $[Fe_{3-}Ow3_6(SO_4)_6]$ clusters and $[FeOw1_6]$ octahedra. And Ow2 atoms which build hydrogen-network-bonded H_2O molecules (H_2Ow2) which are placed in channels running parallel to the a axis (in cages made by channel's intersection) occupy positions which can be compared to the corners of a flattened octahedron and there can be distinguished two bonding-scheme types for this Ow2 atoms, i.e. two hydrogen-bonded network variants around the H_2Ow2 molecules [13].

Rietveld refinement of the coquimbite structure [14] on a sample from the Richmond mine, Redding, California, proved that there is, together with the Al-for-Fe substitution on Fe3 site, also a minor Al-for-Fe substitution on the Fe1 site. Although there is a possibility of a wide range of continuous replacement of the Fe^{3+} by other ions of similar radius, such as especially aluminium, without modifying the structural type, on increasing the Al content beyond a certain limit, a structural rearrangement of the phase occurs, leading to the new mineral species aluminocoquimbite $AlFe^{3+}(SO_4)_3 \cdot 9H_2O$ [15–17]. Mineral coquimbite is polytypic with paracoquimbite, a rhombohedral mineral (space group $R\bar{3}$) [18]. These two minerals, i.e. two layer-like crystal structures differ in layer stacking sequences, with a repeat distance of 8.5 Å between structurally identical but spatially transposed layers.

Approximately 370 sulphate-mineral species are known to exist in nature and they are found in a variety of geological settings, including volcanic, hydrothermal, evaporitic, and chemical-weathering environments [19]. A problem in identification of such minerals with techniques like an X-ray diffraction arrives when closely related minerals are found in paragenetic relationship [20]. So, vibrational spectroscopic techniques are applicable in identification of such paragenetically related minerals.

2. Experimental procedure

2.1. Samples description and preparation

The mineral coquimbite studied in this work was obtained from the collection of the Geology Department of the Federal University of Ouro Preto, Minas Gerais, Brazil, with sample code SAB-101. The sample is from the Javier Ortega mine, Lucanas Province, Peru.

The sample was gently crushed and the associated minerals were removed under a stereomicroscope Leica MZ4. The coquimbite sample was phase analysed by X-ray diffraction. Scanning electron microscopy (SEM) was applied to support the mineralogical chemical.

2.2. Scanning electron microscopy (SEM)

Coquimbite cleavage fragments were coated with a 5 nm layer of evaporated Au. Secondary Electron and Backscattering Electron
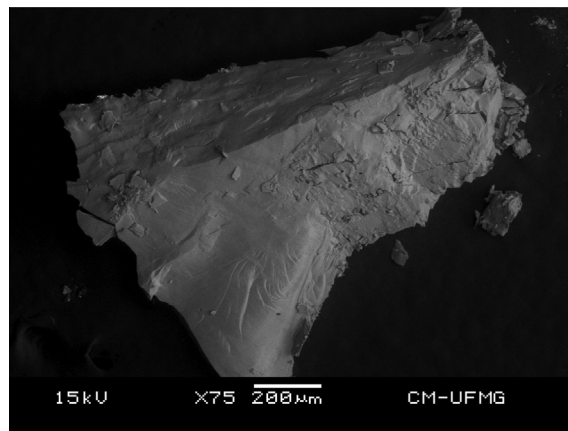

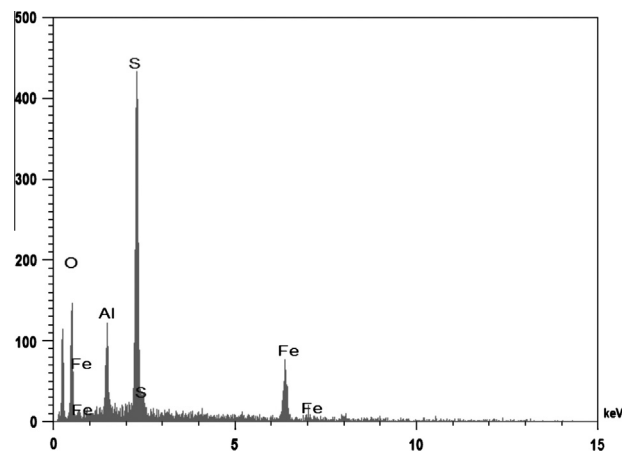**Fig. 1.** Backscattered electron image (BSI) of a coquimbite crystal aggregate up to 0.5 mm in length.
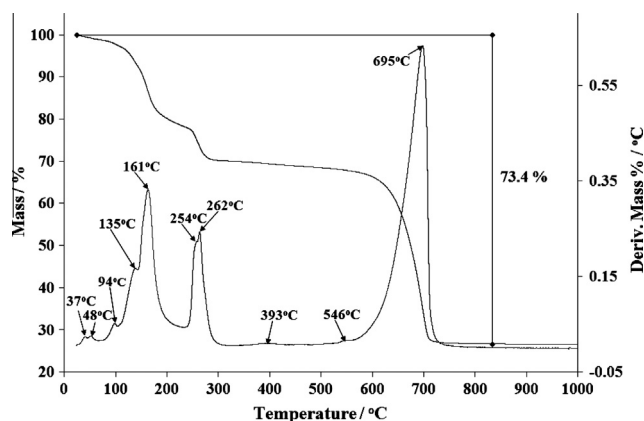

Fig. 2. EDS analysis of coquimbite.

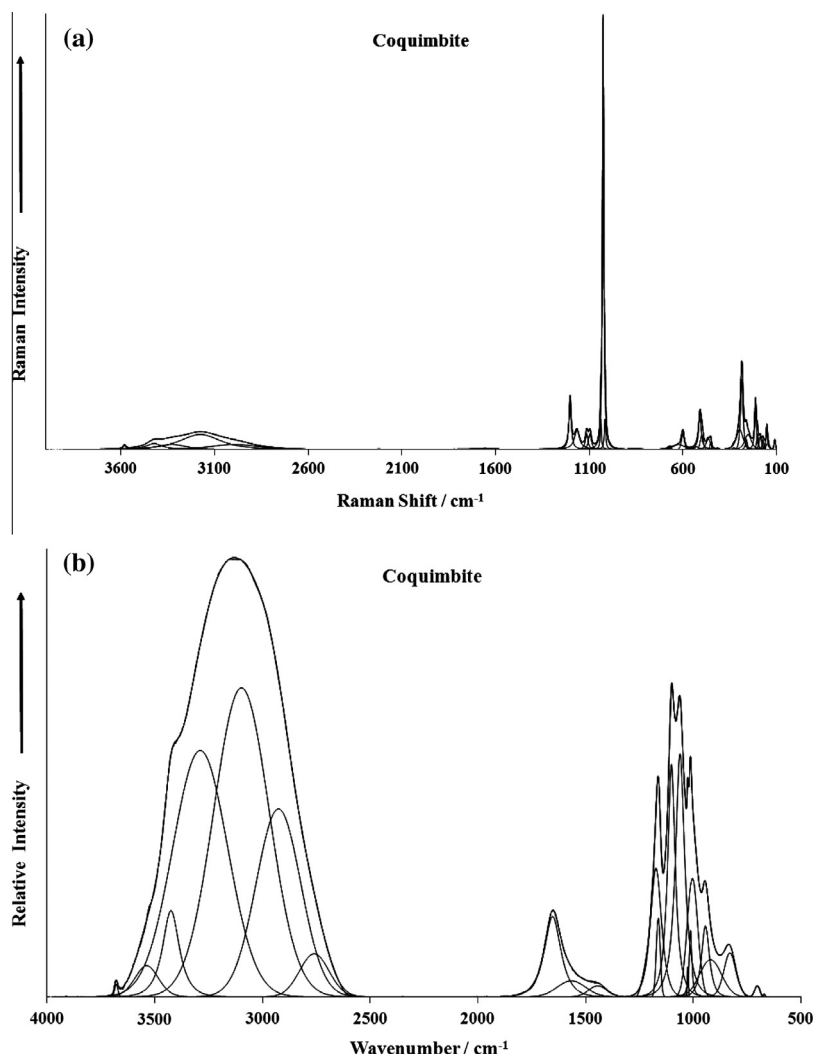**Fig. 3.** Thermal analysis of coquimbite.

Fig. 4. (a) Raman spectrum of coquimbite (upper spectrum) over the 100–4000 cm^{-1} spectral range and (b) infrared spectrum of coquimbite (lower spectrum) over the 500–4000 cm^{-1} spectral range.

images were obtained using a JEOL JSM-6360LV equipment. Qualitative and semi-quantitative chemical analyses in the EDS mode were performed with a ThermoNORAN spectrometer model Quest and were applied to support the mineral characterization.

2.3. Thermogravimetric analysis – TG/DTG

Thermogravimetric analysis of the coquimbite mineral were obtained by using TA Instruments Inc. Q50 high-resolution TGA operating at a 10 °C/min ramp with data sample interval of 0.50 s/pt from room temperature to 1000 °C in a high-purity flowing nitrogen atmosphere (100 cm^3/min). A mass of about 28.0 mg of finely ground dried sample was heated in an open platinum crucible.

2.4. Raman spectroscopy

Crystals of coquimbite were placed on a polished metal surface on the stage of an Olympus BHSM microscope, which is equipped with 10×, 20×, and 50× objectives. The microscope is part of a Renishaw 1000 Raman microscope system, which also includes a monochromator, a filter system and a CCD detector (1024 pixels). The Raman spectra were excited by a Spectra-Physics model 127 He–Ne laser producing highly polarised light at 633 nm and collected at a nominal resolution of 2 cm^{-1} and a precision of

Table 1
Table of the Raman and infrared bands and their assignments.

Raman peak position (cm^{-1})	Infrared peak position (cm^{-1})	Band assignment
3580	3678	OH stretching
3422	3536	
3327	3424	Water stretching
3176	3288	
2994	3096	
1661	1651	Water bending
1201	1172	SO_4^{2-} ν_3
1165	1161	Antisymmetric stretching
1113	1100	
1095	1060	
1037		
1025	1024	SO_4^{2-} ν_1 symmetric stretching
1015	1011	
	1002	
	942	Water librational
	828	
673	701	
620	668	
599		
525		SO_4^{2-} ν_4 bending

(continued on next page)

Table 1 (continued)

Raman peak position (cm^{-1})	Infrared peak position (cm^{-1})	Band assignment
508		
498		
463		SO_4^{2-} ν_2 bending
451		
414		
321		Metal–oxygen stretching
284		
260		Lattice vibrations
251		
211		
201		
186		
172		
164		
151		
141		
108		

±1 cm^{-1} in the range between 200 and 4000 cm^{-1}. Repeated acquisitions on the crystals using the highest magnification (50×) were accumulated to improve the signal to noise ratio of the spectra. Raman Spectra were calibrated using the 520.5 cm^{-1} line of a silicon wafer. The Raman spectrum of at least 10 crystals was collected to ensure the consistency of the spectra.

2.5. Infrared spectroscopy

Infrared spectra were obtained using a Nicolet Nexus 870 FTIR spectrometer with a smart endurance single bounce diamond ATR cell. Spectra over the 4000–525 cm^{-1} range were obtained by the co-addition of 128 scans with a resolution of 4 cm^{-1} and a mirror velocity of 0.6329 cm/s. Spectra were co-added to improve the signal to noise ratio.

Spectral manipulation such as baseline correction/adjustment and smoothing were performed using the Spectracalc software package GRAMS (Galactic Industries Corporation, NH, USA). Band component analysis was undertaken using the Jandel 'Peakfit' software package that enabled the type of fitting function to be selected and allows specific parameters to be fixed or varied accordingly. Band fitting was done using a Lorentzian-Gaussian cross-product function with the minimum number of component bands used for the fitting process. The Gaussian–Lorentzian ratio was maintained at values greater than 0.7 and fitting was undertaken until reproducible results were obtained with squared correlations of r^2 greater than 0.995.
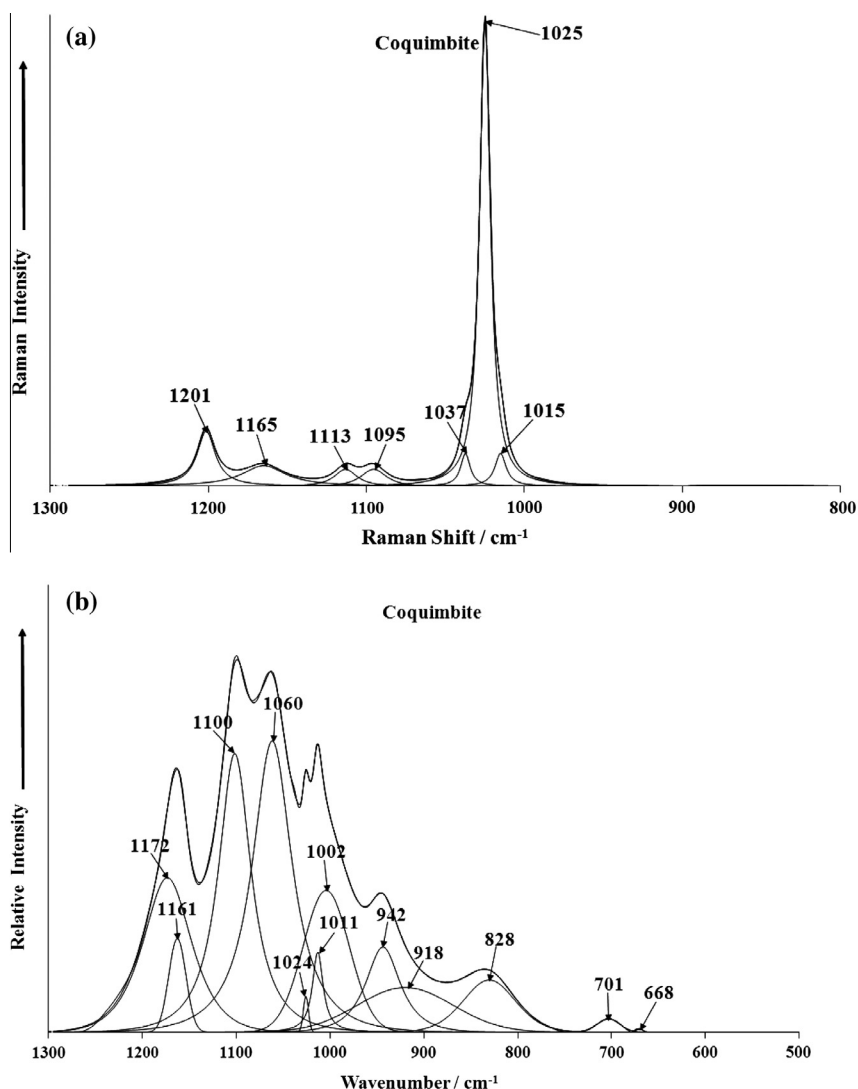

Fig. 5. (a) Raman spectrum of coquimbite (upper spectrum) in the 800–1300 cm^{-1} spectral range and (b) infrared spectrum of coquimbite (lower spectrum) in the 500–1300 cm^{-1} spectral range.
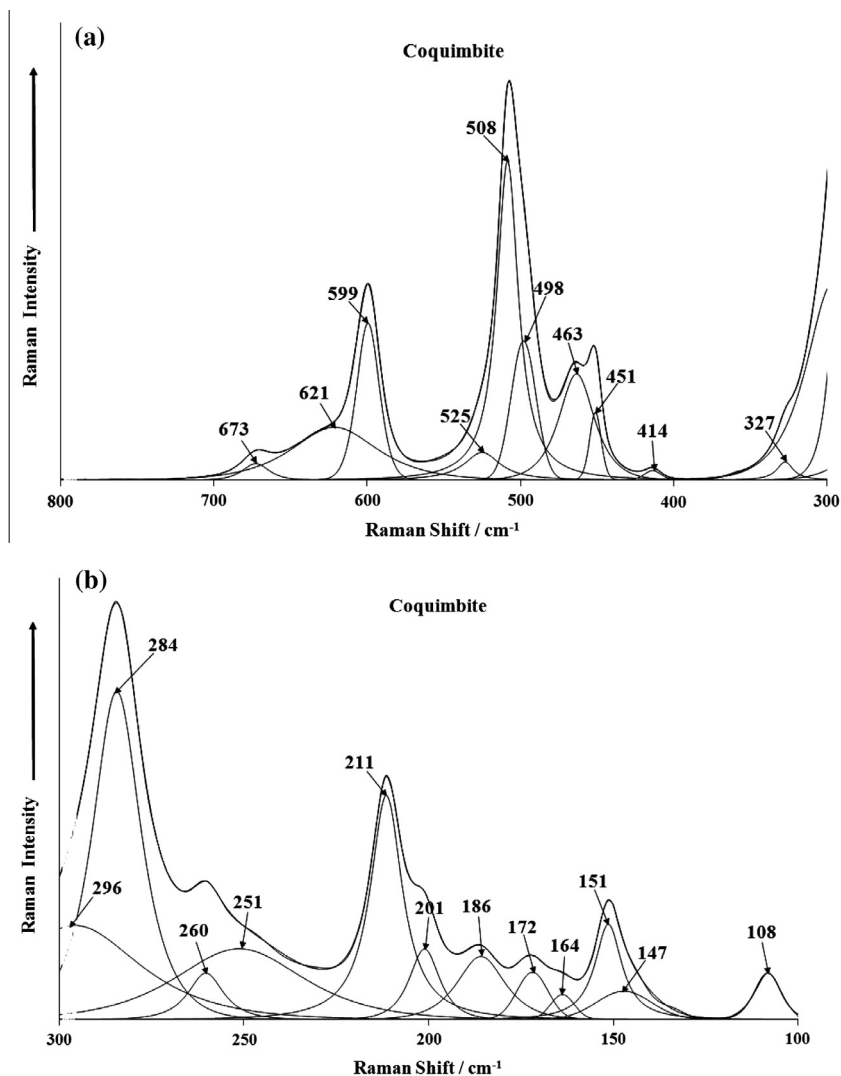
Fig. 6. (a) Raman spectrum of coquimbite (upper spectrum) in the 300–800 cm^{-1} spectral range and (b) Raman spectrum of coquimbite (lower spectrum) in the 100–300 cm^{-1} spectral range.

3. Results and discussion

### 3.1. Chemical characterization

The BSI image of coquimbite sample studied in this work is shown in Fig. 1. Qualitative and semi-quantitative chemical composition shows a Fe and Al sulphate phase. The chemical analysis is represented as an EDS spectrum in Fig. 2. On the basis of semiquantitative chemical analyses the chemical formula was calculated as $(Fe^{3+}_{1.37}, Al_{0.63})_{\sum 2.00}(SO_4)_3 \cdot 9H_2O$.

3.2. Thermal analysis

The thermal analysis of coquimbite is illustrated in Fig. 3. To date, there have been no thermal analytical studies of coquimbite and related minerals [21,22]. There have been some differential thermal analysis study of a very wide range of sulphates from some years past [23]. The TG curve shows a total mass loss of ∼73.4% on heating to 1000 °C and is in agreement with the stoichiometric content of H$_2$O and SO$_3$ that correspond to 74.0 wt%. A significant number of decomposition steps are observed according to the DTG curve in Fig. 3. Small mass loss steps are found at 37, 48 and 94 °C. These mass los steps may be attributed to the loss of

adsorbed water. Further mass loss steps are observed at 135, 161, 254 and 262 °C. These mass loss steps are assigned to the loss of water in stages. Two minor mass losses are found at 393 and 546 °C. A very large mass loss occurs at 695 °C and is assigned to the mass loss of SO$_3$ due to sulphate decomposition. The total mass loss of water according to the given formula is 34.76% and the mass loss of sulphate as SO$_3$ equals 34.73%. Thus the theoretical total mass loss is 69.5%. Thus the difference between the theoretical mass loss and the observed mass loss is 3.9% which is attributed to the loss of adsorbed water.

In the temperature range of 25–100 °C, is observed a mass loss of about 5.2%. The accepted formula by the IMA is $Fe^{3+}_2(SO_4)_3 \cdot 9H_2O$. This mass loss is attributed to the loss of adsorbed water, according to the equation:

$$Fe^{3+}_2(SO_4)_3 \cdot 9H_2O \rightarrow Fe^{3+}_2(SO_4)_3 \cdot 9H_2O + H_2O$$
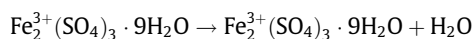
In the temperature range of 500–700 °C a mass loss of 30.43%. A strong exothermic reaction is observed at 641.4 °C. This mass loss is attributed to the loss of sulphate.

$$Fe^{3+}(SO_4)_3 \rightarrow Fe_2O_3 + SO_3.$$ According to this reaction the mass loss of 36% would be predicted based upon the formula $Fe^{3+}_2(SO_4)_3 \cdot 9H_2O$. A mass loss of 30.43% is observed for this step.
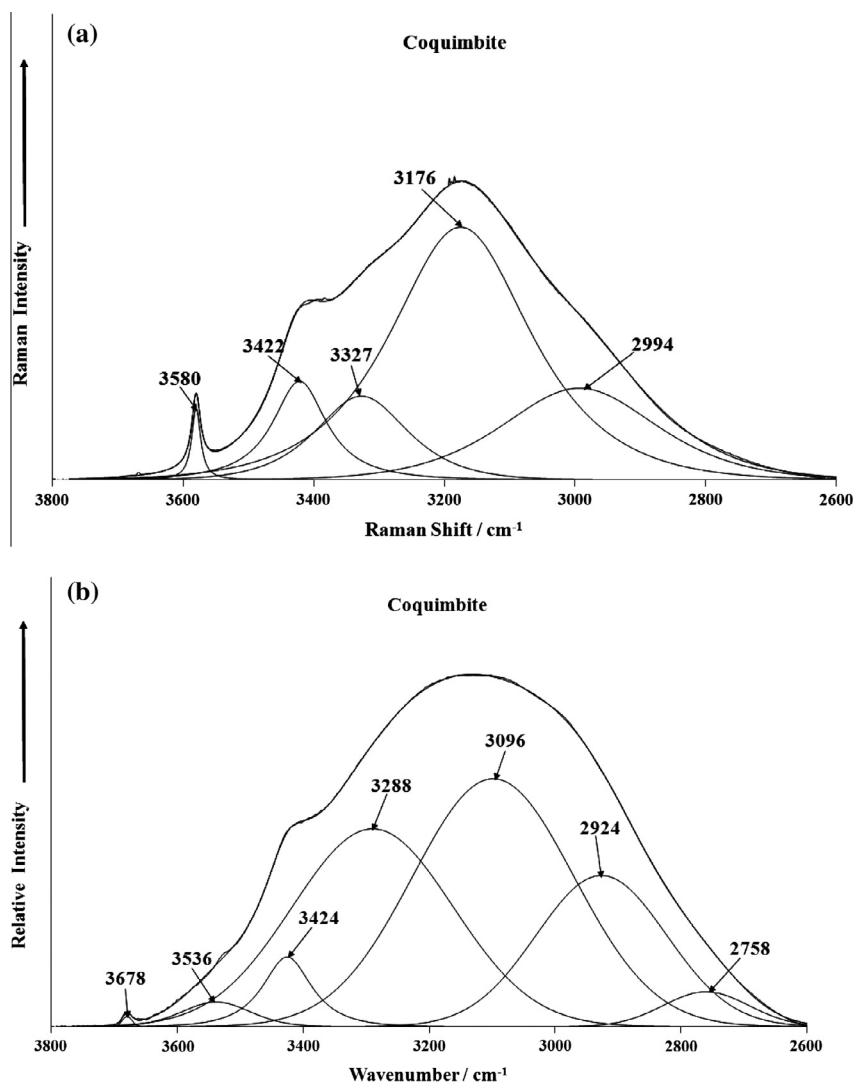
Fig. 7. (a) Raman spectrum of coquimbite (upper spectrum) in the 2600–3800 cm^{-1} spectral range and (b) infrared spectrum of coquimbite (lower spectrum) in the 2600–3800 cm^{-1} spectral range.

3.3. Vibrational spectroscopy

Coquimbite as well as other iron sulphate minerals, were already investigated using NIR spectroscopy [20] and mid-infrared emission spectroscopy [24]. For NIR 6400–7400 cm^{-1} spectral region, spectrum of mineral coquimbite was characterized by overlap of the first HOH fundamentals and the HOH combination bands, and mineral showed intense bands at 6918 and 6646 cm^{-1}. In NIR 4000–5500 cm^{-1} spectral region, bands were observed for coquimbite at 5214, 5144, 5066, 5010 and 4838 cm^{-1}. In the high wavenumber region (7500–1100 cm^{-1}) iron (III) minerals, and so did coquimbite, showed no bands [20]. Early mid-infrared spectroscopic studies have shown that the aqueous sulphate anion (SO$_4$)$^{2-}$ produces four infrared absorption features at ~1105, ~983, ~611, and ~450 cm^{-1} (corresponding to the antisymmetric stretch, ν_3; symmetric stretch, ν_1; asymmetric bend, ν_4; symmetric bend ν_2, respectively) of which only ν_3 and ν_4 are infrared active [24,25]. These vibrations are modified when the sulphate anion is present within a solid-state medium, such as a mineral with a repeating molecular order, resulting in the potential appearance of all four sulphate vibrational modes in the spectrum [24]. In mid-infrared emission spectroscopy investigations, spectra of sample containing both, coquimbite and paracoquimbite showed two clear ν_3 features at 1180 and 1100 cm^{-1}; where the

shape of the 1100 cm^{-1} band suggested that there may be another weaker ν_3 band at slightly lower frequency. There were also a strong ν_1 feature present at 1013 cm^{-1}, three bands at 685, 650, and 975 cm^{-1}, and two ν_2 features at 480 and 443 cm^{-1}, with strong lattice modes occurring at <350 cm^{-1} [24].

The Raman spectrum of coquimbite over the 100–4000 cm^{-1} spectral range is reported in Fig. 4a. This figure shows the position and relative intensity of each Raman band. The spectrum may be subdivided into sections depending upon the type of vibration being analysed. The infrared spectrum of coquimbite in the 500–4000 cm^{-1} spectral region is illustrated in Fig. 4b. This spectrum shows the position and relative intensity of the infrared bands. This spectrum may be subdivided into subsections based upon the vibrational spectroscopic region. The results of the Raman spectroscopic analysis are summarised in Table 1. This Table shows the peak positions of the Raman and infrared bands and their assignment.

3.4. Raman spectroscopy in the 800–1400 cm^{-1} spectral range

The Raman spectrum of coquimbite over the 800–1300 cm^{-1} spectral range is provided in Fig. 5a. The spectrum is dominated by an intense Raman band at 1025 cm^{-1} and is assigned to the SO$_4^{2-}$ ν_1 symmetric stretching mode. Two shoulder bands are
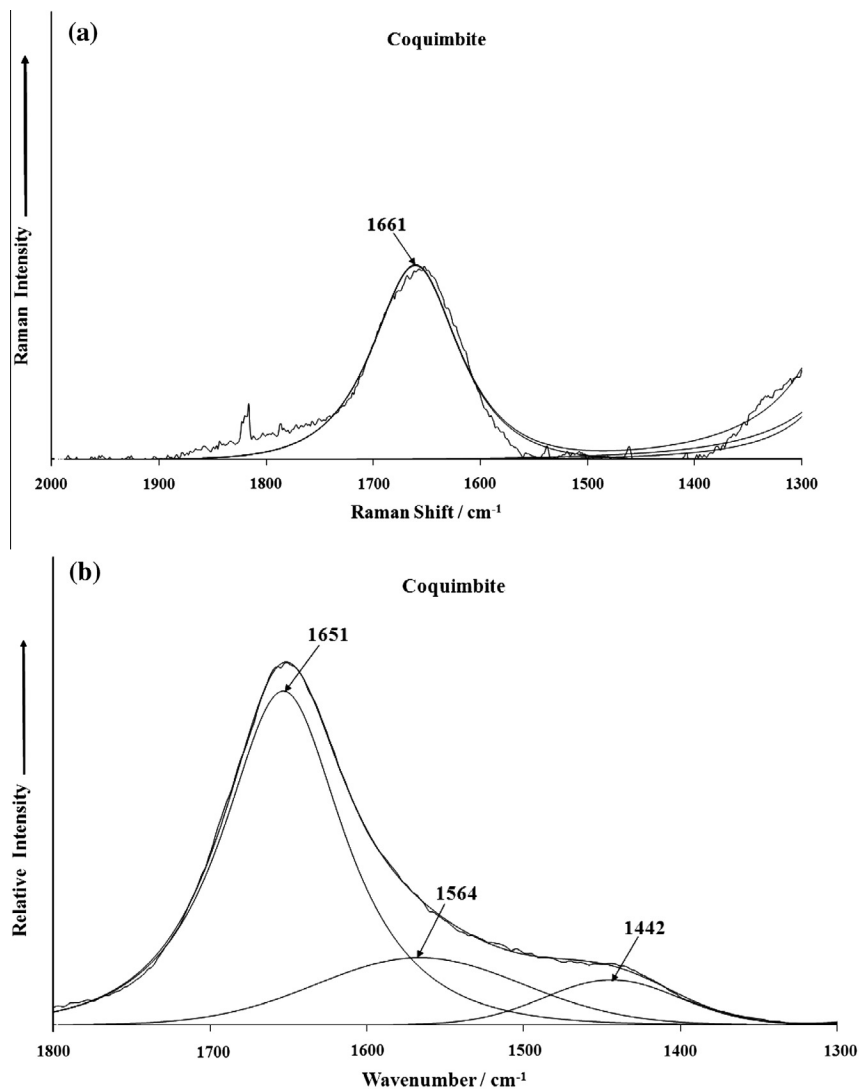
Fig. 8. (a) Raman spectrum of coquimbite (upper spectrum) in the 1300–2000 cm^{-1} spectral range and (b) infrared spectrum of coquimbite (lower spectrum) in the 1300–1800 cm^{-1} spectral range.

observed at 1015 and 1037 cm^{-1}. Four low intensity bands observed at 1095, 1113, 1165 and 1201 cm^{-1} are attributed to the SO$_4^{2-}$ ν_3 antisymmetric stretching modes.

3.5. Infrared spectroscopy in the 500–1300 cm^{-1} spectral range

The infrared spectrum of coquimbite in the 500–1300 cm^{-1} spectral range is given in Fig. 5b. The spectrum shows complexity with a significant number of overlapping bands. The infrared bands recognised at 1060, 1100, 1161 and 1172 cm^{-1} are assigned to the SO$_4^{2-}$ ν_3 antisymmetric stretching modes. The infrared bands at 1011 and 1024 cm^{-1} are attributed to the SO$_4^{2-}$ ν_1 symmetric stretching mode.

3.6. Raman spectroscopy in the 300–800 cm^{-1} and in 100–300 cm^{-1} spectral ranges

The Raman spectrum of coquimbite in the 300–800 cm^{-1} spectral range is shown in Fig. 6a. The Raman spectrum in the 100–300 cm^{-1} spectral range is provided in Fig. 6b. The complexity of the antisymmetric stretching region is reflected in the spectra of the ν_2 bending region. A very intense Raman band is observed at 508 cm^{-1} with additional Raman bands at 414, 451, 463 and

498 cm^{-1}. These bands are assigned to the ν_2 bending modes. Multiple bands are observed in the 400–500 cm^{-1} region for many minerals and are attributed to the ν_2 bending modes. These multiple bands in this ν_2 spectral region are in harmony with the multiple bands observed in the ν_3 spectral region. These multiple bands may occur for several reasons one of which is the reduction of symmetry of the sulphate anion and secondly the fact that not all the sulphate anions are equivalent in the coquimbite structure. A comparison may be made with other sulphate bearing minerals. Bands are observed at 479, 443 and 408 cm^{-1} for cyanotrichite, at 450 and 430 cm^{-1} for devilline, 498 and 471 cm^{-1} for glaucocerinite, at 475, 445 and 421 cm^{-1} for serpierite and at 475 and 449 for ktenasite. For the mineral amarantite, a very intense Raman band is observed at 409 cm^{-1} with additional bands at 399, 451 and 491 cm^{-1}.

The Raman bands at 599, 621 and 673 cm^{-1} are assigned to the sulphate ν_4 bending modes. The observation of multiple bands in this spectral region is in accordance with a reduction in symmetry of the sulphate anion in the coquimbite structure. A comparison may be made with the vibrational spectra of amarantite. A series of low intensity Raman bands for amarantite found at 543, 602, 622 and 650 cm^{-1} are assigned to the ν_4 bending modes. The Raman spectrum of ktenasite shows a single peak in the ν_4 region

at 604 cm^{-1}. The Raman spectrum of devilline shows two low intensity bands at 668 and 617 cm^{-1}; cynaotrichite two overlapping bands at 594 and 530 cm^{-1}; the Raman spectrum of glaucocerinite shows two bands at 694, 613 and 555 cm^{-1}. The complexity of the symmetric and antisymmetric bending region shows a reduction in symmetry for these complex sulphate minerals. Raman spectra of the mineral phases for this region are different, and each phase has its own characteristic spectrum. The observation of multiple bands supports the concept of a reduction in symmetry of sulphate in the coquimbite structure. The Raman spectrum in the far low wavenumber region is shown in Fig. 6b. An intense Raman band at 284 cm^{-1} is assigned to FeO stretching vibrations. Other bands in this spectral region are simply described as lattice vibrations.

3.7. Raman spectroscopy in the 2600–3800 cm^{-1} spectral range

The Raman spectrum of coquimbite over the 2600–3800 cm^{-1} spectral range is displayed in Fig. 7a. The infrared spectrum over this spectral range is given in Fig. 7b. Both spectra are broad with several overlapping bands. The Raman spectrum shows well resolved Raman bands at 2994, 3176, 3327, 3422 and 3580 cm^{-1}. These bands are assigned to the water stretching vibrations. The bands are less well resolved in the infrared spectrum. Infrared bands are noted at 2758, 2924, 3096, 3288, 3424, 3536 and 3678 cm^{-1}. It is likely that the sharp Raman band at 3580 cm^{-1} is attributable to OH stretching vibrations.

3.8. Raman spectroscopy in the 1300–2000 cm^{-1} spectral range

The Raman spectrum of coquimbite over the 1300–2000 cm^{-1} spectral range is shown in Fig. 8a. This spectrum shows a broad Raman band at 1661 cm^{-1}. This band is assigned to the water bending mode. The position of this band supports the concept of very strongly hydrogen bonded water in the coquimbite structure. The position of the water bands in both the Raman and infrared spectra shows that water is strongly hydrogen bonded in the coquimbite structure. Raman and infrared bands below say 4000 cm^{-1} are indicative of strongly hydrogen bonded water. Bands above 3400 cm^{-1} are indicative of weakly hydrogen bonded water in the coquimbite structure.

4. Conclusions

The techniques of electron microscopy, thermogravimetry and vibrational spectroscopy have been combined to determine the chemistry of the mineral coquimbite. Chemical analysis using an electron probe shows qualitatively that only Fe and S are present. On the basis of semiquantitative chemical analyses, the chemical formula was calculated as $(Fe^{3+}_{1.37}, Al_{0.63})_{\sum 2.00} (SO_4)_3 \cdot 9H_2O$.

The TG curve shows a total mass loss of ~73.4% on heating to 1000 °C in agreement with the stoichiometric content of H_2O and SO_3 that correspond to 74.0 wt%.

Thermogravimetry proves the thermal decomposition of coquimbite takes place in a series of four major steps at 135,

161, 254 and 262 °C. A very large mass loss occurs at 695 °C and is assigned to the mass loss of SO_3 due to sulphate decomposition.

Raman spectroscopy is a very powerful tool for the study of sulphate minerals. In this work we have used vibrational spectroscopy to study the mineral coquimbite, a mineral found in evaporate deposits and land surfaces with extreme aridity. Multiple antisymmetric stretching bands are observed as well as multiple bending modes suggesting a reduction in symmetry of the sulphate in the coquimbite structure.

References

[1] J.W. Anthony, R.A. Bideaux, K.W. Bladh, M.C. Nichols, Handbook of Mineralogy,, vol. V, Borates, Carbonates, Sulfates., Mineral Data Publishing, Tucson, 2003.
[2] H. Rose, Annal. Phys. Chem. 27 (1833) 309–319.
[3] J.F.A. Breithaupt, Arnoldische Buchhandlung, Dresden and Leipzig, 1841.
[4] A. Arzruni, Zeit. Kryst. Min. 3 (1879) 516–524.
[5] G. Linck, Zeit. Kryst. Min. 15 (1889) 1–28.
[6] C. Palache, H. Berman, C. Frondel, Dana's system of mineralogy, 7th edition ed., 1951.
[7] A. Kovacs, Foldtani Kozlony 127 (1998) 353–370.
[8] J.H. Bernard, J. Hyršl, Granit, Prague, 2006.
[9] J. Hyršl, Miner. Welt 3 (2010) 68–71.
[10] D.M.C. Huminicki, F.C. Hawthorne, Can. Min. 38 (2000) 1425–1432.
[11] M. Mrose, D.E. Appleman, Zeit. Kryst. Min. 117 (1962) 16–36.
[12] J.-H. Fang, P.D. Robinson, Am. Min. 55 (1970) 1534–1539.
[13] C. Giacovazzo, S. Menchetti, F. Scordari, Rendiconti 49 (1970) 129–140.
[14] J. Majzlan, A. Navrotsky, R.B. McCleskey, C.N. Alpers, Eur. J. Min. 18 (2006) 175–186.
[15] F. Demartin, C. Castellano, C.M. Gramaccioli, I. Campostrini, Can. Min. 48 (2010) 323–333.
[16] F. Demartin, C. Castellano, C.M. Gramaccioli, I. Campostrini, Can. Min. 48 (2010) 1465–1468.
[17] F. Demartin, C. Castellano, C.M. Gramaccioli, I. Campostrini, Min. Mag. 74 (2010) 375–377.
[18] P.D. Robinson, J.H. Fang, Am. Min. 56 (1971) 1567–1572.
[19] F.C. Hawthorne, S.V. Krivovichev, P.C. Burns, The Crystal Chemistry of Sulfate Minerals, Sulfate Minerals: Crystallography, Geochemistry, and Environmental, significance ed., Mineralogical Society of America, Chantilly, Virginia, 2000.
[20] R.L. Frost, R.-A. Wills, W. Martens, M. Weier, B.J. Reddy, Spectrochim. Acta 62A (2005) 42–50.
[21] R. Scharizer, Zeit. Kryst. Min. 56 (1921) 353–385.
[22] R. Scharizer, Zeit. Kryst. Min. 65 (1927) 335–360.
[23] G. Cocco, Periodico di Min. 21 (1952) 103–138.
[24] M.D. Lane, Am. Min. 92 (2007) 1–18.
[25] K. Nakamoto, Infrared and Raman Spectra of Inorganic and Coordination Compounds, Wiley & Sons, New York, 1986.